Related edge	Kinematic endpoint
l^+l^- edge	$(m_{ll}^{\max})^2 = (\tilde{\xi} - \tilde{l})(\tilde{l} - \tilde{\chi})/\tilde{l}$
l^+l^-q edge	$(m_{llq}^{\max})^2 = \begin{cases} \max\left[\frac{(\tilde{q}-\tilde{\xi})(\tilde{\xi}-\tilde{\chi})}{\tilde{\xi}}, \frac{(\tilde{q}-\tilde{l})(\tilde{l}-\tilde{\chi})}{\tilde{l}}, \frac{(\tilde{q}\tilde{l}-\tilde{\xi}\tilde{\chi})(\tilde{\xi}-\tilde{l})}{\tilde{\xi}\tilde{l}}\right] \\ \text{except for the special case in which } \tilde{l}^2 < \tilde{q}\tilde{\chi} < \tilde{\xi}^2 \\ \text{and } \tilde{\xi}^2\tilde{\chi} < \tilde{q}\tilde{l}^2 \text{ where one must use } (m_{\tilde{q}} - m_{\tilde{\chi}_1^0})^2. \end{cases}$
Xq edge	$(m_{Xq}^{\max})^2 = X + \frac{(\tilde{q}-\tilde{\xi})}{2\tilde{\xi}}\left[\tilde{\xi} + X - \tilde{\chi} + \sqrt{(\tilde{\xi} - X - \tilde{\chi})^2 - 4X\tilde{\chi}}\right]$
l^+l^-q threshold	$(m_{llq}^{\min})^2 = \begin{cases} [\ \ 2\tilde{l}(\tilde{q} - \tilde{\xi})(\tilde{\xi} - \tilde{\chi}) + (\tilde{q} + \tilde{\xi})(\tilde{\xi} - \tilde{l})(\tilde{l} - \tilde{\chi}) \\ \ \ -(\tilde{q} - \tilde{\xi})\sqrt{(\tilde{\xi} + \tilde{l})^2(\tilde{l} + \tilde{\chi})^2 - 16\tilde{\xi}\tilde{l}^2\tilde{\chi}}\ \ ]/(4\tilde{l}\tilde{\xi}) \end{cases}$
$l^\pm_{\text{near}}q$ edge	$(m_{l_{\text{near}}q}^{\max})^2 = (\tilde{q} - \tilde{\xi})(\tilde{\xi} - \tilde{l})/\tilde{\xi}$ (unobservable)
$l^\pm_{\text{far}}q$ edge	$(m_{l_{\text{far}}q}^{\max})^2 = (\tilde{q} - \tilde{\xi})(\tilde{l} - \tilde{\chi})/\tilde{l}$ (unobservable)
$l^\pm q$ high-edge	$(m_{lq(\text{high})}^{\max})^2 = \max\left[(m_{l_{\text{near}}q}^{\max})^2, (m_{l_{\text{far}}q}^{\max})^2\right]$
$l^\pm q$ low-edge	$(m_{lq(\text{low})}^{\max})^2 = \min\left[(m_{l_{\text{near}}q}^{\max})^2, (\tilde{q} - \tilde{\xi})(\tilde{l} - \tilde{\chi})/(2\tilde{l} - \tilde{\chi})\right]$
$\tilde{l}\bar{\tilde{l}}$ edge	$\Delta M^{\max} = (m_{\tilde{l}}^2 - m_{\tilde{\chi}_1^0}^2)/(2m_{\tilde{l}})$

Table 5.2: *The absolute kinematic endpoints of invariant mass quantities formed from decay chains of the types mentioned in the text for known particle masses. The following shorthand notation has been used:* $\tilde{\chi} = m^2_{\tilde{\chi}_1^0}, \tilde{l} = m^2_{\tilde{l}_R}, \tilde{\xi} = m^2_{\tilde{\chi}_2^0}, \tilde{q} = m^2_{\tilde{q}}$ *and* X *is* m_h^2 *or* m_Z^2 *depending on which particle participates in the "branched" decay. The positions of endpoints are derived in Appendix D.*

For completeness, the same table includes the positions of the unobservable near- and far-edges. Note that although the position of the high-edge is just the higher of $m^{\max}_{l_{\rm near}q}$ and $m^{\max}_{l_{\rm far}q}$, the position of the low-edge has a more interesting form. This asymmetry arises because it is not always kinematically possible for the invariant mass of the lepton-quark pair coming from the lower of the near- and far-distribution to approach $\min\left[m^{\max}_{l_{\rm near}q}, m^{\max}_{l_{\rm far}q}\right]$ arbitrarily closely, while simultaneously requiring that this invariant mass is less than that of the other lepton-quark pair.

5.7.6 Dislepton production, $M_{T2}^{\max}(\chi)$, ΔM and the $\tilde{l}\bar{\tilde{l}}$ edge

One of the novel parts of this analysis concerns the introduction of ΔM, a variable designed to better constrain the slepton-LSP mass difference.

It is easiest to describe ΔM in terms of a related variable, $M_{T2}(\chi)$ proposed by the author (in collaboration) in [28].

$M_{T2}(\chi)$ may be used to study events where:

- the event contains two identical two-body decays (i.e. $X \to Y a_1 a_2$ followed by $a_1 \to b_1 c_1$ and $a_2 \to b_2 c_2$),
- $m_A = m_{a_1} \equiv m_{a_2}$ is unknown,
- $m_C = m_{c_1} \equiv m_{c_2}$ is unknown,
- $m_B = m_{b_1} \equiv m_{b_2}$ is known,
- particles of type c are undetectable,
- the longitudinal momentum of the incoming particles is also unknown, and
- Y does not contain any unobservable particles such as neutrinos.

In such cases, the variable provides a kinematic constraint on the masses of particles of type a and type c. In this analysis, $M_{T2}(\chi)$ will be applied to dislepton events of the form $pp \rightarrow Y\tilde{l}_R^{\pm}\tilde{l}_R^{\mp} \rightarrow Yl^{\pm}l^{\mp}\tilde{\chi}_1^0\tilde{\chi}_1^0$ (Figure 5.4) using the assignment $a = \tilde{l}$, $b = e/\mu$ and $c = \tilde{\chi}_1^0$. These events are used to constrain $m_{\tilde{l}}$ and $m_{\tilde{\chi}_1^0}$ in the following way:

Suppose, for the moment, that the mass of the neutralino were known, and denoted by $m_{\tilde{\chi}}$ (the numbers in $\tilde{\chi}_1^0$ have been dropped to avoid confusion with subscripts indicating which decay the neutralino came from). Then, if it were possible to observe the momenta of each neutralino, and correctly identify its associated lepton, it would be possible to compute the invariant mass of either slepton using the exact relation:

$$m_{\tilde{l}}^2 = m_l^2 + m_{\tilde{\chi}}^2 + 2(E_T^l E_T^{\tilde{\chi}} \cosh(\Delta y) - \mathbf{p}_T^l \cdot \mathbf{p}_T^{\tilde{\chi}}) \tag{5.9}$$

where $E_T^l = \sqrt{{\mathbf{p}_T^l}^2 + m_l^2}$, $E_T^{\tilde{\chi}} = \sqrt{{\mathbf{p}_T^{\tilde{\chi}}}^2 + m_{\tilde{\chi}}^2}$ and Δy is the difference between the rapidities (see Appendix C) of the lepton and the neutralino. This definition includes the lepton masses for completeness, although these are neglected in all computations. Of course, observing the neutralinos is impossible at ATLAS, so the difference in rapidities, Δy, will certainly not be known. Nevertheless, using the fact that $\cosh \Delta y \geq 1$, it is possible to make the reduced claim:

$$m_{\tilde{l}}^2 \geq m_T^2(\mathbf{p}_T^l, \mathbf{p}_T^{\tilde{\chi}}, m_{\tilde{\chi}}) \equiv m_l^2 + m_{\tilde{\chi}}^2 + 2(E_T^l E_T^{\tilde{\chi}} - \mathbf{p}_T^l \cdot \mathbf{p}_T^{\tilde{\chi}}), \tag{5.10}$$

or even the stronger claim:

$$m_{\tilde{l}}^2 \geq \max\{m_T^2(\mathbf{p}_T^{l_1}, \mathbf{p}_T^{\tilde{\chi}_1}, m_{\tilde{\chi}}), m_T^2(\mathbf{p}_T^{l_2}, \mathbf{p}_T^{\tilde{\chi}_2}, m_{\tilde{\chi}})\} \tag{5.11}$$

using both of the decays. But neither $m_T^2(\mathbf{p}_T^l, \mathbf{p}_T^{\tilde{\chi}}, m_{\tilde{\chi}})$ nor the right hand side of (5.11) is an observable quantity, as each relies upon knowledge of the transverse components of the momenta of each neutralino. Under the prevailing assumptions, the only thing known about the neutralinos is the *sum* of their transverse momenta, given by the missing momentum of the event:

$$\not{\mathbf{p}}_T = \mathbf{p}_T^{\tilde{\chi}_1} + \mathbf{p}_T^{\tilde{\chi}_2}. \tag{5.12}$$

Although the form of the splitting (5.12) is not known, it is possible to turn the right hand side of (5.11) into a quantity $M_{T2}^2(m_{\tilde{\chi}})$ which *is* observable, by trying all possible splittings. This motivates the definition:

$$M_{T2}^2(m_{\tilde{\chi}}) \equiv \min_{\not{\mathbf{p}}_1 + \not{\mathbf{p}}_2 = \not{\mathbf{p}}_T} \left[\max\left\{ m_T^2(\mathbf{p}_T^{l_1}, \not{\mathbf{p}}_1, m_{\tilde{\chi}}), m_T^2(\mathbf{p}_T^{l_2}, \not{\mathbf{p}}_2, m_{\tilde{\chi}}) \right\} \right], \tag{5.13}$$

which must therefore satisfy

$$m_{\tilde{l}}^2 \geq M_{T2}^2(m_{\tilde{\chi}}). \tag{5.14}$$

In [28], the authors note that it *is* kinematically possible for equality to be reached in (5.14), and that this occurs when $\Delta y_1 = \Delta y_2 = 0$ and $\mathbf{v}_T^{l_1} - \mathbf{v}_T^{\tilde{\chi}_1}$ is parallel (note: not anti-parallel) to $\mathbf{v}_T^{l_2} - \mathbf{v}_T^{\tilde{\chi}_2}$, where $\mathbf{v}_T = \mathbf{p}_T / E_T$. Thus, by construction, $M_{T2}(m_{\tilde{\chi}})$ has the property that, for a large enough number of signal events in a perfect detector,

$$M_{T2}^{\max}(m_{\tilde{\chi}_1^0}) \equiv \max_{\text{events}} \left[M_{T2}(m_{\tilde{\chi}_1^0}) \right] = m_{\tilde{l}}, \tag{5.15}$$

which is equivalent to saying that the endpoint of the $M_{T2}(m_{\tilde{\chi}})$ distribution occurs at the slepton mass.

Note that up to this point it has been necessary to assume knowledge of the neutralino mass, $m_{\tilde{\chi}} \equiv m_{\tilde{\chi}_1^0}$, which is a little unfair, given that it is one of the quantities which the analysis seeks to determine. Formally, then, the M_{T2} distribution is not a single distribution, but a family of distributions: one for each possible value of the neutralino mass. For example; suppose it is proposed that the neutralino mass is equal to "χ" (not necessarily close to the correct value). This would motivate plotting the distribution of $M_{T2}(\chi)$, generated from dislepton events under the hypothesis that the neutralino mass may be taken to be χ rather than $m_{\tilde{\chi}}$ in definition (5.13). Having plotted this distribution, the location $M_{T2}^{\max}(\chi)$ of its endpoint could be ascertained, and the interpretation of $M_{T2}^{\max}(\chi)$ would be "the slepton mass favoured by the data given the assumed neutralino mass".

Thus the overall result obtained from a full set of $M_{T2}(\chi)$ distributions, is a function $M_{T2}^{\max}(\chi)$, describing the most favoured slepton mass as a function of neutralino mass χ.

In Section D.7 of the Appendix it is shown that the function $M_{T2}^{\max}(\chi)$ is in fact dependent on only one unknown parameter $p > 0$; namely the modulus of the three-momentum of the lepton (or the neutralino) in the rest frame of the slepton. In general p is given by

$$p^2 = \frac{m_{\tilde{l}}^4 + m_{\tilde{\chi}_1^0}^4 + m_l^4 - 2(m_{\tilde{l}}^2 m_{\tilde{\chi}_1^0}^2 + m_{\tilde{l}}^2 m_l^2 + m_{\tilde{\chi}_1^0}^2 m_l^2)}{4 m_{\tilde{l}}^2}. \tag{5.16}$$

In Section D.7 the general form of the dependence of $M_{T2}^{\max}(\chi)$ upon p is shown to be:

$$M_{T2}^{\max}(\chi) = \sqrt{m_l^2 + p^2} + \sqrt{\chi^2 + p^2}. \tag{5.17}$$

Significantly, (5.17) may be inverted for arbitrary χ yielding:

$$p^2 = \frac{\tilde{L}^4 + \chi^4 + m_l^4 - 2(\tilde{L}^2\chi^2 + \tilde{L}^2 m_l^2 + \chi^2 m_l^2)}{4\tilde{L}^2} = \text{"independent of } \chi\text{"}, \tag{5.18}$$

where $M_{T2}^{\max}(\chi)$ has been abbreviated to $\tilde{L}$. The reader is encouraged to compare (5.18) with (5.16). The result (5.18) is important for two reasons. Firstly it tells us that we no longer need to worry about choosing a particular value of χ in the region of $m_{\tilde{\chi}_1^0}$, and secondly it shows us that p from (5.16) is the quantity which $M_{T2}^{\max}(\chi)$ is *really* constraining. In fact, the most elegant way of extracting p from $M_{T2}(\chi)$ measurements actually *exploits* the freedom to choose an arbitrary value of χ. Paradoxically, the best choice for χ turns out to be neither 0 nor $m_{\tilde{\chi}_1^0}$ (which one might have expected from the original definition of χ) but is in fact m_l. Using this value one may define the quantity $\Delta M \geq 0$ by

$$(\Delta M)^2 \equiv \frac{1}{4}\left(M_{T2}(m_l)\right)^2 - m_l^2 \qquad (5.19)$$

and thereby obtain from (5.17) the significant result that:

$$\Delta M^{\max} = p = p(m_{\tilde{l}}, m_{\tilde{\chi}_1^0}, m_l). \qquad (5.20)$$

As a consequence of this important result, it is distributions of ΔM which are chosen to be plotted to extract model independent information from dislepton events.[h] The result (5.20) shows us that the location of the ΔM edge (i.e. $\Delta M^{\max}$) is a direct measumenet of p given by (5.16).

Thus far, the only approximation which has been made was the presumption that transverse slepton boosts have a negligible effect on the prediction for $\Delta M^{\max}$ given in (5.20). Within this thesis, however, there is additionally a motivation for neglecting the lepton masses:

In order to maximise the size of the signal, the analysis presented in this thesis will seek both e^+e^- and $\mu^+\mu^-$ events. The presence of the lepton mass in (5.20) (or equivalently in the definition of p) suggests that one ought to analyse events with different

---

[h] It should be noted that montecarlo studies suggest that the evaluation of $M_{T2}(\chi)$ at values of χ different than $m_{\tilde{\chi}_1^0}$ can introduce a slight dependence of the edge position upon the maximum transverse boost attained by the sleptons. For example, it has been observed that in a situation where *both* sleptons are able to be emitted collinearly and with transverse momenta of 20 GeV (or 100 GeV or 1000 GeV), then the value of $\Delta M^{\max}$ predicted by (5.20) for heavy (left) sleptons at S5 would underestimate th true value by about 2% (or 8% or 14%). As expected, transverse boosts are observed to have no effect on $M_{T2}^{\max}(m_{\tilde{\chi}_1^0})$. The precise reason for this effect is still under investigation, but within this analysis the effect may safely be ignored for two reasons. Firstly, dislepton production is threshold dominated, and so sleptons typically have small transverse momenta. Secondly, and more importantly, the cut limiting jet activity to "at most one with $p_T < 40$ GeV" puts a strong constraint on the momentum available for the sleptons to recoil against. This restricts the washing out of the edge to a 2% effect, which is far less than the order 10% error on the edge position due to statistics. In situations where the effect cannot be neglected, systematic error could be minimised by evaluating $M_{T2}(\chi)$ at the best avaliable guess for $m_{\tilde{\chi}_1^0}$.

leptons differently. Note, however, that in cases where the $\Delta M^{\max}$ is observed to lie at a mass much in excess of m_l, one may immediately deduce that $m_l \ll p$. The assumption $m_l \ll p$, together with definition (5.16), may be used to show that $m_l \ll m_{\tilde{l}} - m_{\tilde{\chi}_1^0}$, which itself permits p to be expanded in terms of $\epsilon = m_l/(m_{\tilde{l}} - m_{\tilde{\chi}_1^0})$ as follows:

$$\Delta M^{\max} = p = p_{\text{approx}} \left\{ 1 - \frac{m_{\tilde{l}}^2 + m_{\tilde{\chi}_1^0}^2}{(m_{\tilde{l}} + m_{\tilde{\chi}_1^0})^2} \epsilon^2 - \frac{2 m_{\tilde{l}}^2 m_{\tilde{\chi}_1^0}^2}{(m_{\tilde{l}} + m_{\tilde{\chi}_1^0})^4} \epsilon^4 + O(\epsilon^6) \right\} \tag{5.21}$$

where

$$p_{\text{approx}} \equiv \frac{m_{\tilde{l}}^2 - m_{\tilde{\chi}_1^0}^2}{2 m_{\tilde{l}}}. \tag{5.22}$$

This shows that when $\Delta M^{\max} \gg m_l$, then one may take $\Delta M^{\max}$ to be really just a measurement of p_{approx} given by (5.22).

The ΔM distributions arising from two test models examined in this thesis do in fact happen to satisfy $\Delta M^{\max} \gg \max[m_e, m_\mu]$ at the 100 GeV $\gg$ 100 MeV level, and so within this thesis $\Delta M^{\max}$ is taken to be equivalent to p_{approx} as defined in (5.22). This means that within this part of the analysis it is safe to take the leptons to be massless and to analyse both the e^+e^- and the $\mu^+\mu^-$ events together.

To summarise the analysis of the dislepton edge:

- The distributions which will be plotted and whose edges will be identified, will be distributions of ΔM.
- The observation that $\Delta M^{\max} \gg m_\mu$ for the models under study permits us to: neglect lepton masses, analyse both e^+e^- and $\mu^+\mu^-$ events together, and interpret $\Delta M^{\max}$ as a measurement of $p_{\text{approx}} = (m_{\tilde{l}}^2 - m_{\tilde{\chi}_1^0}^2)/(2m_{\tilde{l}})$.
- Were the analysis to be performed at another point where $\Delta M^{\max}$ was much less than (or order) m_l, then the analysis could still proceed, but it would no longer be possible to treat $\Delta M^{\max}$ as a measurement of p_{approx}. $\Delta M^{\max}$ would instead

constrain p. Beacuse p depends on m_l, one would have to consider e^+e^- events separately from $\mu^+\mu^-$ events.

The ΔM edge can thus be included in the analysis to provide an additional constraint on the slepton and neutralino masses. The name 'ΔM' is chosen because, to first order, $\Delta M^{\max} \approx p_{\text{approx}}$ is well approximated by the slepton/neutralino mass difference provided that the slepton is not *much* heavier than the neutralino.

In practice the ΔM edge can be distorted by the finite resolution of the detector or missing energy from soft underlying events. Additionally, standard model (SM) backgrounds provide constraints on minimum detectable slepton/neutralino mass differences (see Section **??**) **XXX FIX REFERENCE!! XXX**. However the most important factor to control is the ability to correctly identify which production processes are contributing to an observed $\Delta M(\chi)$ edge – particularly since it is possible to have multiple edges in the *non* standard model contributions to $\Delta M(\chi)$ distributions. At S5, for example, where both the right- and left-sleptons are lighter than at O1 (see Table 5.1), both $\tilde{l}_R^+\tilde{l}_R^-$ and $\tilde{l}_L^+\tilde{l}_L^-$ events pass the cuts, and two edges are generated. The edge coming from the (lighter) right-slepton falls well under the SM background and so is not measurable, while the (heavier) left-slepton still has a cross section for pair-production high enough to let it form a good edge of its own at $\Delta M(m_{\tilde{\chi}_1^0}) = m_{\tilde{l}_L} - m_{\tilde{\chi}_1^0}$. It is important that this edge is not mistaken for one produced by $\tilde{l}_R$, so methods are needed to dismiss it. Discussion of these issues are delayed until Section **??** XXX FIX REFERENCE!! XXX.

5.7.7 Notes concerning interpretation of endpoint positions

Were all squarks to have the same mass, then (with perfect detector resolution and with infinite statistics) the endpoints of the edges listed above would be found at the positions listed above and summarised in Table 5.2. Note that these positions depend on four unknown parameters, namely the masses of the squark, the slepton and the two neutralinos participating in each decay. The mass of the lightest higgs boson also appears, but it will be assumed that the higgs mass will already be known or will be obtained by other methods (e.g. [14]) to within 2%.

In a more realistic "non-degenerate squark masses" scenario, every distribution with a squark related edge will actually be a superposition of many underlying distributions (one for each squark mass), each having its edge at a slightly different location. This results in some smearing of the edges, even before detector effects (resolutions, acceptances, jet energy calibrations etc.) are taken into account.

It is not possible to measure each of the squark masses separately. Consequently the quantity $m_{\tilde{q}}$ in Table 5.2 will, after being obtained from the "smeared" edges, represent a squark mass *scale* rather than a specific squark mass. In all squark related edges, except the l^+l^-q threshold, the contribution to the outermost part of each edge is provided by the heaviest squarks. In the case of the l^+l^-q threshold, the "true" endpoint is set by the lightest squark. However, if (as at O1 and S5) the other eleven squarks are much heavier (see Table 5.1), it is easier to measure the contribution coming from them. A strong correlation between $m_{\tilde{q}}$ and the mass of the heaviest squark would therefore be expected.

More work would be required to fully understand the "theoretical" systematic errors including the use of a full simulation of the expected edge positions. Better edge models than those used later in this analysis will definitely be needed in order to permit measurements of edge positions to be better correlated with functions of the particle masses. Other sources of systematic errors which require further analysis are the detector effects mentioned above, combinatorial backgrounds near the edges and possible cut biases. Such systematic errors can only meaningfully be studied when real data are available.

It has already been said that, within this thesis, it will be assumed that the above investigations could be performed so as to leave the eventual edge resolutions determined only by statistics and detector resolution. In this analysis, then, all edges are fitted with simple shapes (see Section 5.10.1) with the intention of extracting only an estimate of the *uncertainty* on the edge position, and not to obtain the edge position itself.

5.8 Event generation and pile-up

All events, except those for $q\bar{q} \to W^+W^-$ background processes, were simulated by `HERWIG-6.0` [29]. The W-pair events were generated by `ISAJET-7.42` [30].

At high luminosity, approximately 20 minimum bias events ("pile-up" events) are expected to occur in each bunch crossing. No pile-up events were generated for this analysis, but their effects will have been accounted for within the `ATLFAST` simulation, which alters its reconstruction resolutions in the different luminosity environments appropriately. But resolutions are not the only things which change at high luminosity. For example, the number of jets per bunch crossing with more than a given p_T rises with luminosity, but this effect would not be reproduced by the simulation method described so far. Consequently all cuts which are expected to perform under high luminosity must be checked for susceptibility to the effects which `ATLFAST` does not consider.

Except where stated otherwise, **XXX IS THIS TRUE? XXX,** events were generated and studied in batches corresponding to 100 fb^{-1} in the high luminosity environment. This is expected to correspond to approximately one year of high luminosity running.

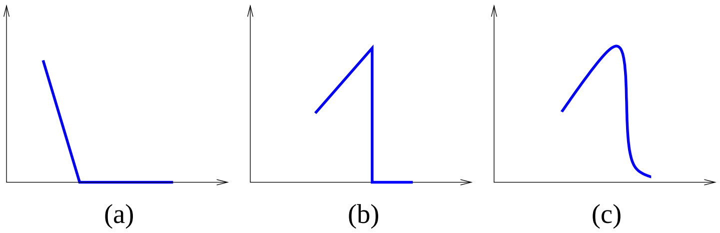

Figure 5.7: *Line-shapes used for fits to the mass distributions. Shape (a) (or its reflection in the vertical axis) is the standard "straight line" used to extract the* l^+l^-q *edge,* $l^\pm q$ *high-edge,* $l^\pm q$ *low-edge and* l^+l^-q *threshold resolutions. Shape (b) models the expected shape of the sharp* l^+l^- *edge in the absence of detector effects. The* l^+l^- *edge is actually fitted with shape (c), which is identical to (b) except that it is smeared with a Gaussian resolution whose width is a free parameter of the fit.*

similar quality at O1 (see Figure 5.6: a, b and d). In addition, plots c1 and c2 in Figures 5.5 and 5.6 display the $m_{lq(\mathrm{high})}$ and $m_{lq(\mathrm{low})}$ distributions generated from the modified $l^\pm q$ edge cuts also listed above.

The distributions seen at S5 and O1 are broadly similar to each other. The most obvious difference between the two sets of data is the peak at the Z mass present in Figure 5.6a but absent in Figure 5.5a. This peak comes from direct $\tilde{\chi}_2^0 \to \tilde{\chi}_1^0 Z \to \tilde{\chi}_1^0 l^+ l^-$ decays, which have a branching fraction of 39% at O1 compared with 0.65% at S5. The most common direct neutralino decay mode at S5 is through the h_0 (65%) of which only a tiny proportion (0.02%) decay to the two light leptons as the partial decay width $\Gamma(h_0 \to f f)$ goes approximately as m_f^2. Scenarios in which the l^+l^- edge happens to coincide with the Z peak would require special treatment and are not considered here.

It has already been mentioned that the primary reason for plotting these distributions is not to recover the locations of the edges themelves, but to get an idea of the limit which finite statistics imposes on the resolution of each endpoint. These errors will serve as the foundation for assessing the method as a whole, under the assumption that systematic effects are small in comparison to statistical errors.

In order to extract estimates for the statistical errors on the endpoints, simple fits have been made to the distributions of Figures 5.5 and 5.6. The shapes fitted to the data (see Figure 5.7) and the algorithms for determining the boundaries of the fitted regions have been kept as simple and generic as possible, with the intention of making the fit results both conservative and simple to interpret. Only two shapes were used to fit the edges; a straight line for most edges, and a triangular distribution smeared by a gaussian resolution for the l^+l^- edge. The use of the special method at the l^+l^- edge is justified by the unique step-like nature of its edge (which may not be approximated by a straight line of finite gradient) and also by the fact that the expected shape of the edge is simple to interpret theoretically (see Section 5.7.1) and is unlikely to introduce unwanted model dependence.

To try to avoid bias toward one or either model or toward one or either edge, all the distributions fitted with a *straight line* (ten in total) were fitted by *the same algorithm.* This algorithm was given the tasks of both identifying the range of bins over which to fit, as well as the endpoint of the edge and its gradient. There were a number of inputs to the algorithm common to all distributions, describing "what to look for in an edge" (such as a maximum height which the top part of the edge may reach as a fraction of the height of the bin containing the most events, or a minumum number of events required to be present in each bin over the fit range) but only one input which was permitted to vary from edge to edge; namely the instruction indicating whether to look for a threshold (i.e. left-hand edge) or a forwards edge (i.e. right-hand edge).

The resolutions obtained from the fits to the distributions in Figure 5.5 and Figure 5.6 are listed in Table 5.5.

Given real data, it would be worth putting substantial effort into understanding how detector and physics effects affect the shape of each distribution in turn, particularly in the neighbourhood of each edge. This might significantly improve particle mass resolutions, or at least improve confidence in the errors associated with each edge. But as the events being processed here are entirey synthetic, the fit errors listed in Table 5.5 will be used as they are.

5.10.2 ΔM edge resolution

Determining the likely resolution for the ΔM edge requires a slightly different approach to that used for the "boost invariant" edges above. Whereas the cuts used to obtain the above invariant mass distributions have high SM rejections (primarily due to the presence of at least one high mass $\not{p}_T$ or $M_{\text{effective}}$ requirement), the ΔM cuts cannot be set so hard, primarily because the desired dislepton events have have very little jet activity. (With the dislepton production cross sections typically two orders of magnitude smaller than the squark/gluino production cross sections (Table 5.3) a low efficiency is not affordable.) There are also irreducible SM backgrounds (primarily $W^+W^- \to l^+l^-\nu\bar{\nu}$ and $t\bar{t} \to b\bar{b}W^+W^- \to jjl^+l^-\nu\bar{\nu}$ in cases where jets are below the reconstruction threshold or are outside detector acceptance) which have signatures identical to dislepton events. The smallness of the signal and the presence of these backgrounds would cause problems for naive straight line fitting techniques of the type used above, and so estimation of the edge precision requires the following discussion:

Figure 5.8 shows the ΔM distributions obtained at S5 and O1 after applying the cuts listed in Section 5.9.1 to a 100 fb^{-1} sample of signal dislepton events. Events from lighter sleptons ($\tilde{e}_R$ and $\tilde{\mu}_R$) occupy the unhatched region in each plot, while the events from heavier left-sleptons are cross hatched. It will be noted that events from both light and heavy sleptons succeed in passing the cuts in both models. In principle, then, there are two edges to be observed in each of the models: one for the lighter slepton and one for the heavier. We note, however, that the slepton masses increase, their production is strongly suppressed, and so there are very few heavy slepton events at O1 where there

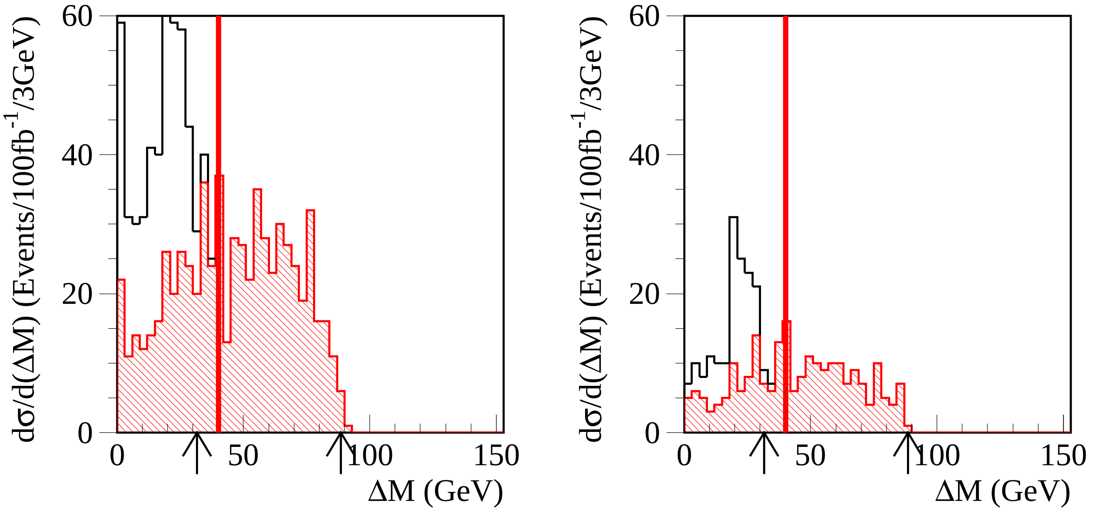

(a) S5, soft cuts

(b) S5, hard cuts

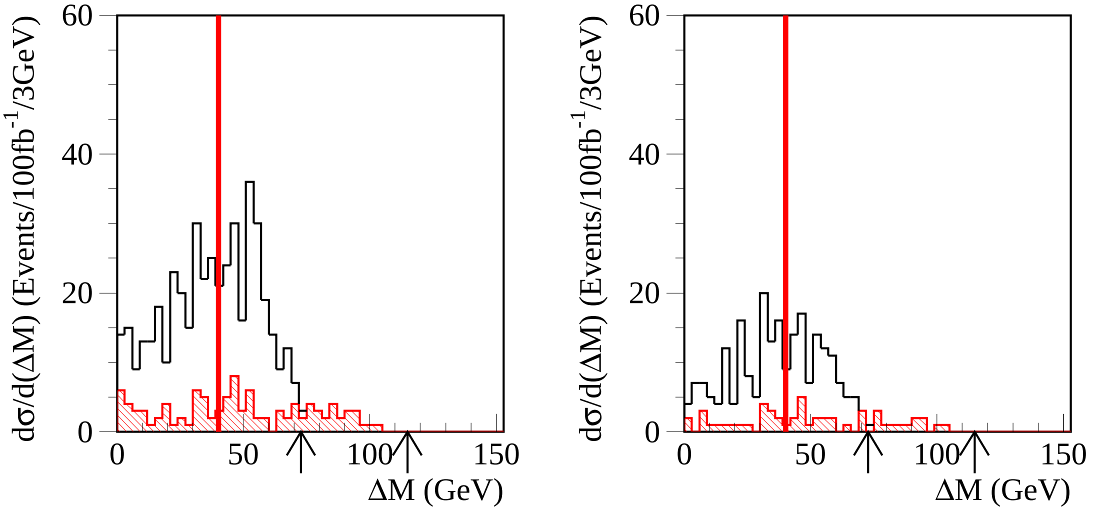

(c) O1, soft cuts

(d) O1, hard cuts

Figure 5.8: *ΔM distributions obtained at S5 and O1 after applying the cuts listed in Section 5.9.1 to a* $100\ \mathrm{fb}^{-1}$ *sample of* $\tilde{e}_R\bar{\tilde{e}}_R$, $\tilde{\mu}_R\bar{\tilde{\mu}}_R$, $\tilde{e}_L\bar{\tilde{e}}_L$ *and* $\tilde{\mu}_L\bar{\tilde{\mu}}_L$ *dislepton events. Events from light right-sleptons (unhatched) are stacked on top of those from heavier left-sleptons (hatched). Only events from OSSF leptons combinations are shown. The plots are generated without OSDF background subtraction, but were it to be performed, no significant differences would be apparent as only 4 (12) signal events are able to pass OSDF soft cuts at S5 (O1). Arrows indicate the values of* $\Delta M^{\max}$ *predicted by theory for the two types of slepton in each model. A red vertical line is drawn through each plot at half the* W *mass.*

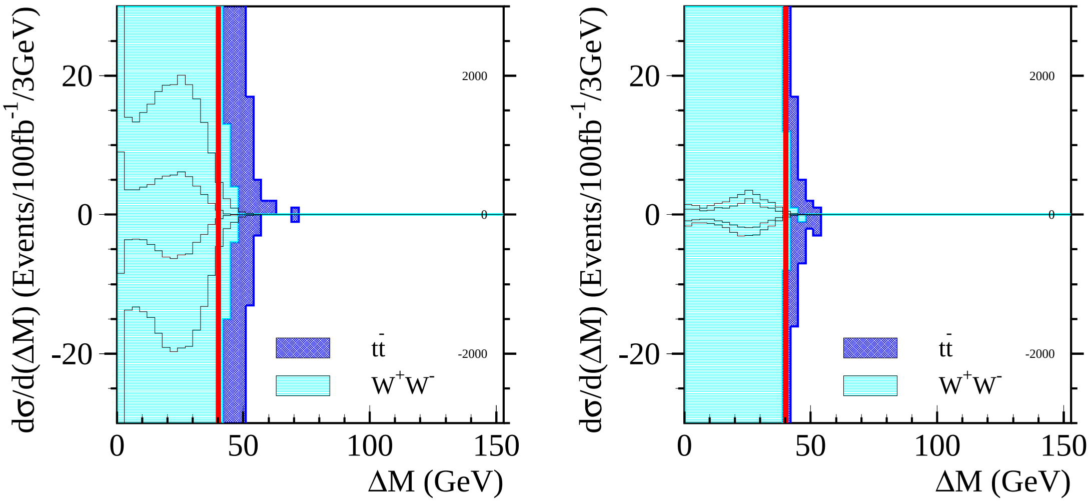

(a) SM backgrounds, soft cuts

(b) SM backgrounds, hard cuts

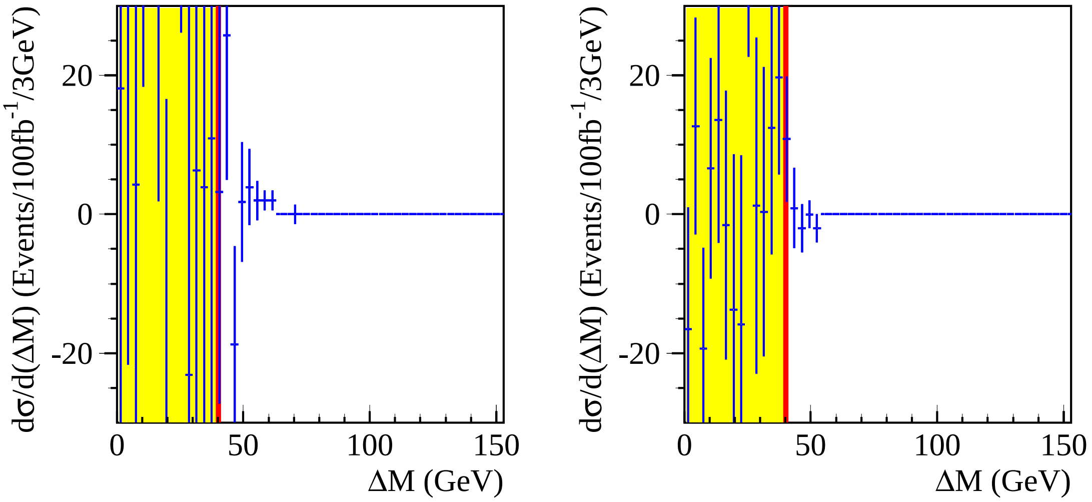

(c) SM (OSSF-OSDF), soft cuts

(d) SM (OSSF-OSDF), hard cuts

Figure 5.9: *SM background to ΔM measurement. The plots above show the ΔM distributions obtained after cuts from* 100 fb^{-1} *of W-pair and $t\bar{t}$ background samples. In (a) and (b), events passing the OSSF cuts are stacked with positive weight, while events passing the OSDF cuts are stacked with negative weight. Because number of events passing cuts in (a) and (b) is very large, the outlines of the stacked histograms are overlapped after being downscaled by a factor of 100 (see scales on right hand side of each plot). Plots (c) and (d) show the result of subtracting the OSDF events passing the cuts from the OSSF events passing the cuts. A red vertical line is drawn through each plot at half the W mass. Plots (c) and (d) are shaded to the left of this line in order to draw attention to the performance of the background subtraction* above *this point.*

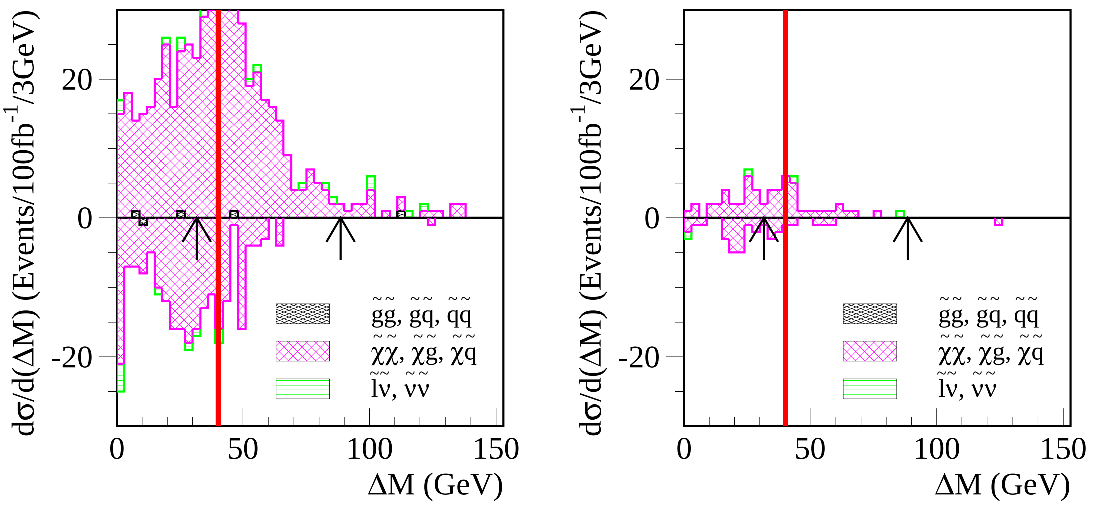

(a) S5, soft cuts

(b) S5, hard cuts

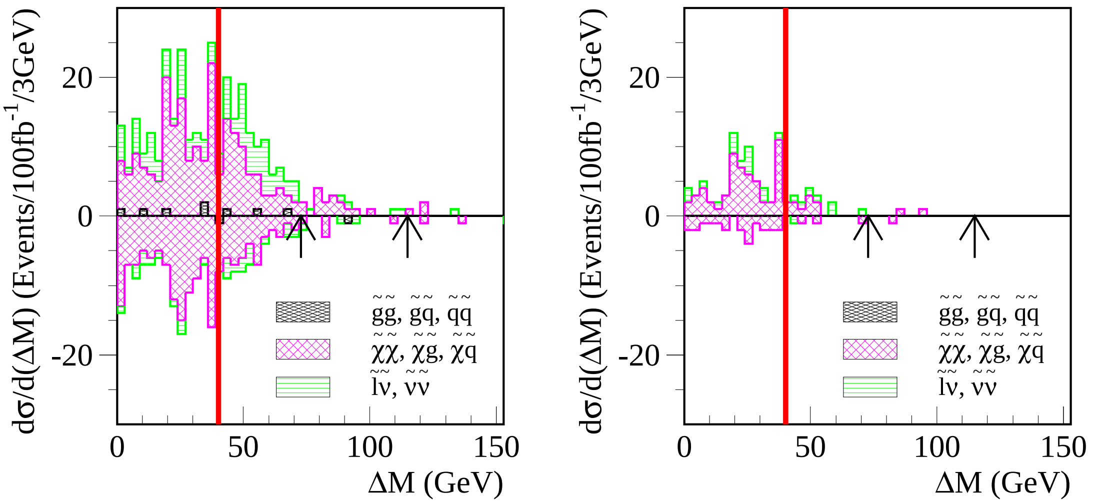

(c) O1, soft cuts

(d) O1, hard cuts

Figure 5.10: *ΔM distributions obtained at S5 and O1 after applying the cuts listed in Section 5.9.1 to the remainder of the supersymmetric cross section not generated for Figure 5.8. Events passing the OSSF cuts are stacked by primary parton pair with positive weight, while events passing the OSDF cuts are stacked with negative weight. A red vertical line is drawn through each plot at half the W mass.*

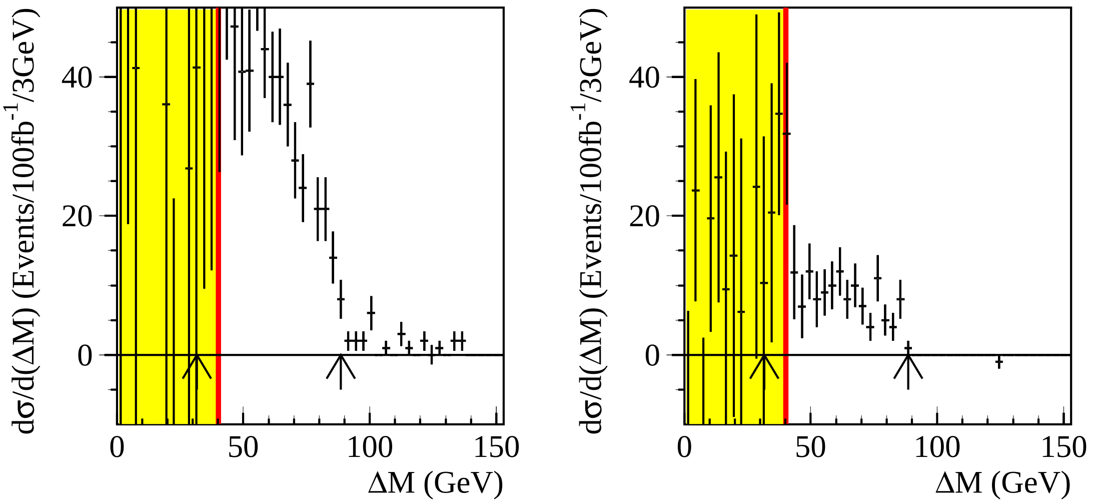

(a) S5, soft cuts

(b) S5, hard cuts

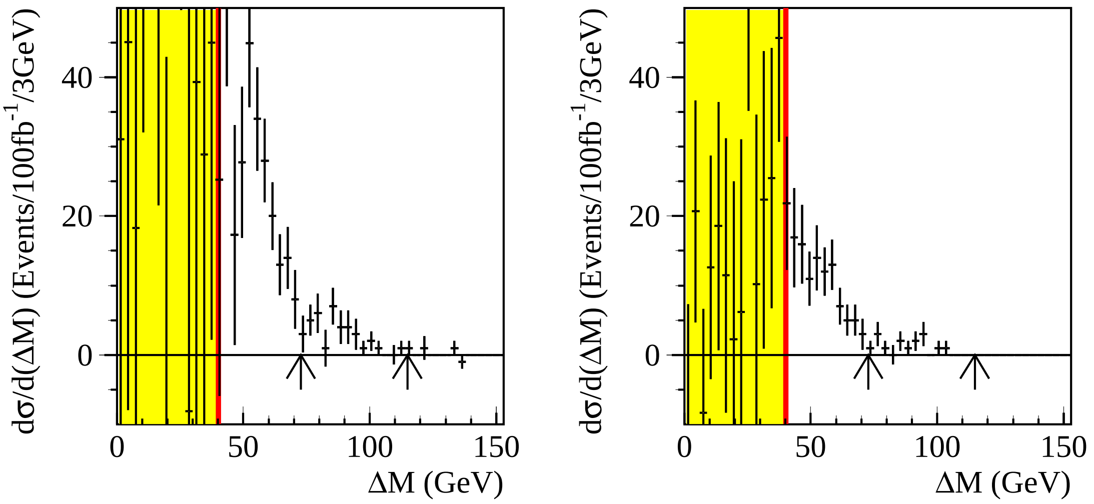

(c) O1, soft cuts

(d) O1, hard cuts

Figure 5.11: *Flavour-subtracted ΔM distributions for combined signal and background at S5 and O1 after applying the cuts listed in Section 5.9.1. A red vertical line is drawn through each plot at half the W mass. Plots are shaded to the left of this line in order to draw attention to the events which reconstruct* above *this point. Compare these plots with those of Figure 5.8 which contain only signal events.*

are in fact none within 10 GeV of the kinematic limit. It is readily observed that at the three remaining edges, where statistics are higher, there is good agreement between the theoretical prediction and the observed endpoint of each distribution.

Looking next at the SM backgrounds in Figure 5.9(a) and Figure 5.9(b) we see that the number of $t\bar{t}$ and W^+W^- events passing the "soft" cuts is about two orders of magnitude larger than the number of signal events passing cuts. Fortunately, although large in number, these events are easy to understand. As the source of leptons and missing energy in these events are not sleptons but W-bosons, we expect the edge of the SM background to fall at half the W mass (as this is the modulus of the three momentum of the decay products of the W in its rest frame). From the "zoomed out" histograms in Figures 5.9(a) and 5.9(b) it may be seen that the W-pair background does indeed have an endpoint at $m_W/2$. The same is true of the $t\bar{t}$ events passing the hard cuts, although under the soft cuts the $t\bar{t}$ edge does begin to wander up to 50 GeV, probably due to the effects of poorer $\not{p}_T$ resolution when more hadronic energy is permitted in events as well as the effect of allowing a larger range of transverse boosts for the W-bosons. Nevertheless, the sheer number of SM events passing both sets of cuts, combined with the finite detector resolution, allows significant numbers of events to reach 50 GeV (hard cuts) or 60 GeV (soft cuts). This leakage threatens to further restrict the minimum position at which a supersymmetric edge in ΔM might be observed. Fortunately, the OSSF SM background may be seen to be well modelled by its OSDF counterpart. Since the signals from dislepton pair production are expected to be purely OSSF (because of lepton-number conservation) there is a strong motivation for using different-family background subtraction. The quality of this subtraction may be seen in Figures 5.9(c) and (d). Across the whole range of $\Delta M > 0$ the SM background is consistent with zero after subtraction. If these Figures are compared with the signal distributions shown in Figure 5.8, it may be seen that after subtraction, the SM backgrounds have been reduced to a level where they are very much less than the signal in all bins above $m_W/2$, except perhaps in the two lowest bins in the case of the soft cuts. It is reasonable to assume, therefore, that in the real experiment; the OSDF ΔM distribution could be used to place limits on the number of OSSF events which, if observed above a given value of ΔM, would provide significant evidence of physics beyond the SM. Beacause of the interplay between signal edge position and signal cross section, one cannot make a definitive statement of the form "if a supersymmetric model has a dislepton edge above X GeV then it will be observable". However, it is clear that observation of dislepton edges below $m_W/2$ is highly unlikely, observation of edges in the range $m_W < \Delta M < 50$ GeV will be possible if the number of signal events is significantly larger than the number of SM background events, and observation of an edge above 50 GeV is likely to be limited only by signal cross section itself. From these considerations we see that the light slepton edge at S5 is rendered unobservable by the presence of the SM background, but that the statuses of the other edges (including those of O1) remain unaffected.

Having looked at the signal and the SM processes, there remains only the supersymmetric backgrounds to consider. Figure 5.10 shows the remaining non-signal events from supersymmetric production processes, after both the OSSF and the OSDF versions of the cuts. We notice here that, with the single exception of the soft cuts at S5, the OSSF distributions are well modelled by the OSDF events passing the same cuts. Even where the background subtraction is not perfect, we again see that the supersymmetric backgrounds remain small in comparison with the signal distributions (see Figure 5.8) and are either absent or constant in the vicinity of the slepton edges. **XXX I'm not too concerned about this, but why would we expect the *unsubtracted* mixed bg at S5 to be quite as large as it is, as after all, the BF for (Ntlino2→Ntlino1 lepton antilepton) is only twice as big at S5 as at O1. Since the excess disappears in the hard cuts, it presumably comes from associated production of NtlinoTwo and (quark or gluon). Persumalbly there is some argument about how the ntlinotwo's gaugino/higggsino components favour its production in**

assoc with the light left-squarks at S5 whereas in O1 they probably only get made with the heavier right-squarks. How about this Peter? XXX

All events (signals and backgrounds) are combined in Figure 5.11 after different-family background subtraction. The reader is encouraged to compare these plots with those from Figure 5.8 showing the desired signal shapes. As expected, all signal shape information is lost to the left of $m_W/2$ due to obliteration by the SM backgrounds. To the right of this point, at least one clear edge is observable in both models (the left-slepton edge at S5, and the right-slepton edge at O1) and in both sets of cuts. The hard cuts are able to suppress the supersymmetric backgrounds to such a degree that there is even compelling evidence at O1 for the existence of *two* edges, although the lack of statistics in the higher edge limits the precision with which the endpoint may be located. By the same token, the lack of a high tail at S5 (under the hard cuts) might be interpreted as evidence that the sailient edge was itself due to the heaviest left-sleptons. These conjectures will not be persued in this thesis, however. It will be sufficient for the analysis in hand to draw the following conservative conclusion from the plots: It will be assumed that where a signal dislepton edge occurs in the range $50\text{ GeV} < \Delta M^{\max} < 100\text{ GeV}$, then the location of the endpoint can be determined using the soft cuts alone to a precision of 10%. The (lowest) edge measured in this way will be referred to as the "principal ΔM edge". At O1 it comes from lighter right-sleptons, while at S5 it comes from heavier left-sleptons.

5.11 Modelling the endpoint measurement process itself

Given the non-trivial relationships between the expected endpoint locations and the sparticle masses, the approach used to evaluate the eventual errors for the reconstructed sparticle masses is non trivial. The approach used in this thesis, consistent with the assumption of negligible systematic error, will require "modelling the endpoint measurement process itself". This will allow mass reconstructions by an "ensemble" of ATLAS experiments to be performed in parallel, the spread of whose measurements will form an estimate of the accuracy obtainable by any one measurement on its own.

Using the fit errors, σ_i, of Table 5.5 as estimates of the statistical error associated with a typical endpoint measurement, the whole process of edge fitting, calibration and endpoint measurement is mimicked using the following prescription:

1. Select n endpoints to "measure".

2. Identify the values $O_i(p_{\mathrm{model}})$ $(i = 1, ..., n)$ which the observables (which is to say endpoint positions) would be expected to take if a perfect measurement could be performed. Clearly the observables would depend on the masses of the sparticles of the model in question, and this is indicated by the functional dependence of the $O_i(p_{\mathrm{model}})$ on the masses, p_{model}.

3. Construct "measured" observables, $\Omega_i^{\mathrm{sm}}(p_{\mathrm{model}})$, by smearing the $O_i(p_{\mathrm{model}})$ according to $\Omega_i^{\mathrm{sm}} = O_i(p_{\mathrm{model}}) + \sigma_i X_i$, where $X_i \sim N(0,1)$ are n random variables from the Normal distribution (with zero mean and unit standard deviation) and σ_i is the anticipated statistical error for the i^{th} observable.

The n observables Ω_i^{sm} may thus be thought of as endpoint locations which *might have been obtained at ATLAS after collection of* 100 fb^{-1} *of data,* were it possible to remove systematic effects. As the generation of the Ω_i^{sm} only required the selection of n random numbers, many such "measurements" can be made very quickly.

5.11.1 Reconstruction of sparticle masses

Given a set of "measured" observables Ω_i^{sm}, sparticle masses are reconstructed by finding the particular set of masses, p_{fit}, which minimises the chi-squared of the fit of the predictions $O_i(p_{\mathrm{fit}})$ to the measurements Ω_i^{sm}.

The main parameters p of the fit are $m_{\tilde{\chi}_1^0}$, $m_{\tilde{l}}$, $m_{\tilde{\chi}_2^0}$ and $m_{\tilde{q}}$. The masses m_h and m_Z also appear as fit parameters, but they are strongly constrained (particularly in the case of the Z) by existing LEP measurements and the expected LHC higgs mass error (0.0077% and 2.0% respectively).

Formally, then, the chi-squared is formulated as:

$$\chi^2(p) = \sum_1^n \frac{\left(\Omega_i^{\mathrm{sm}} - O_i(p)\right)^2}{{\sigma_i}^2}, \tag{5.24}$$

and the results of the fit, p_{fit}, are thus the particular masses which minimise the chi-squared. p_{fit} may be interpreted as "the set of masses most consistent with Ω_i^{sm}", where Ω_i^{sm} are a set of measurements which could have been made by ATLAS after $100\mathrm{fb}^{-1}$ of high luminosity running. In order to determine the accuracy with which this reconstruction can be performed, the above fitting process is repeated many times for different values of the Ω_i^{sm}, so as to observe the spread in the reconstructed masses.

5.12 Basic reconstruction

The role of each edge in the analysis is best demonstrated by an incremental approach, in which edges are incorporated one at a time. The first form of the analysis, including only the l^+l^- edge, the l^+l^-q edge, the $l^\pm q$ high-edge, the Xq edge and the l^+l^-q threshold, might be termed the "basic analysis".

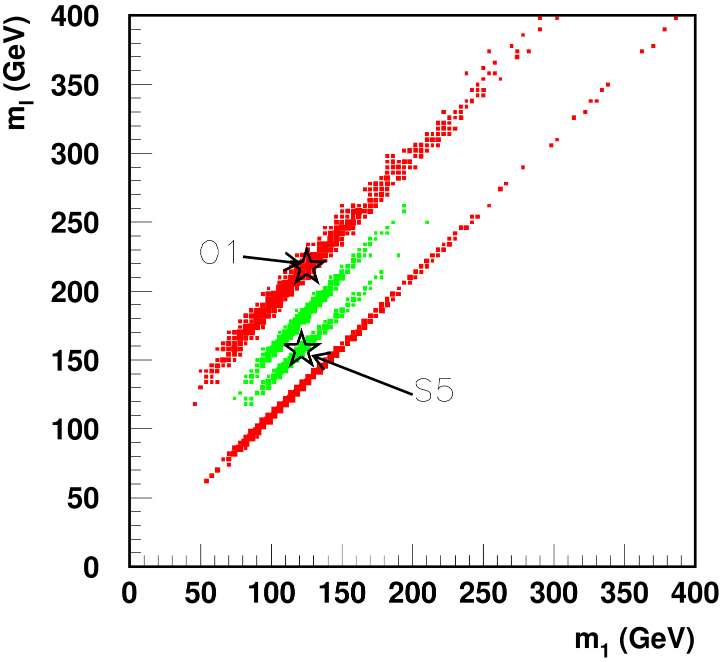

Figure 5.12: *The spread of* $\tilde{l}_R$ *and* $\tilde{\chi}_1^0$ *masses reconstructed by an ensemble of simulated ATLAS experiments, each using the "basic" analysis (see Section 5.12). Reconstructions in which the underlying model was S5 are shown in light green, while the results of reconstruction based on O1 are shown in dark red. The stars indicate the input values of the masses in each of the models.*

Of all the forms of the analysis which will be described here, the basic analysis is the one most similar to that used in [25–27]. Common to both, are the number of edges and the types of particles involved in them. The very important difference between them, however, is that the analysis described here does not presuppose any *special* relationships between the masses of the sparticles in the decay chains, as is evidenced by the generalisations of the l^+l^-q edge and $l^\pm q$ high-edges. As a consequense, the basic analysis does not constrain sparticle masses as much as the original did.

Figure 5.12 shows the spread of $\tilde{l}_R$ and $\tilde{\chi}_1^0$ masses that are reconstructed by use of the basic analysis at the two test models. The two most important features to observe in Figure 5.12 are the doubling up of the reconstructed regions for each model, and the strong positive correlation between reconstructed neutralino and slepton masses. While it is reassuring to see that sparticle masses stand a “fair” chance of being reconstructed in a region close to their input values, it is evidently the case that there are comparably sized regions which are equally consistent with the edge measurements, but which are are not centred on the desired values.

To state the problem more precisely, for each model there appear to be two slepton/neutralino mass differences which are consistent with the measured edge positions. Both mass differences are measured with an error which is tiny in comparison with the error on the overall mass scale, but there is no way of choosing between the two possibilities. It is not surprising that mass differences are better constrained than absolute masses, since the energies available to the visible particles radiated in decay chains are dependent primarily on the mass differences between the invisible sparticles. The unfortunate twofold ambiguity concerning the choice of the *correct* slepton/neutralino mass difference arises as a direct consequence of the generalised treatment of the l^+l^-q edge and $l^\pm q$ high-edge. It is clear that more work must now be done to constrain the masses better.

Before demonstrating an improved analysis, it is interesting to note that without the l^+l^-q threshold the situation would be even worse, as shown in Figure 5.13. In this figure one can see that, in addition to false solutions being present, the absolute sparticle masses are not even bounded above. Indeed, only at S5 could there even be said to be *lower* bounds for the sparticle masses. It should be noted that in this “cut-down” version of the basic analysis, the number of edge constraints is equal to the number of free sparticle masses (four), so independent constraints should to leave the masses entirely determined (no degrees of freedom). That this does not happen, is proof that the constraints coming from the edges are not completely independent. To first order they are principally constraints on the mass differences, and they only constrain

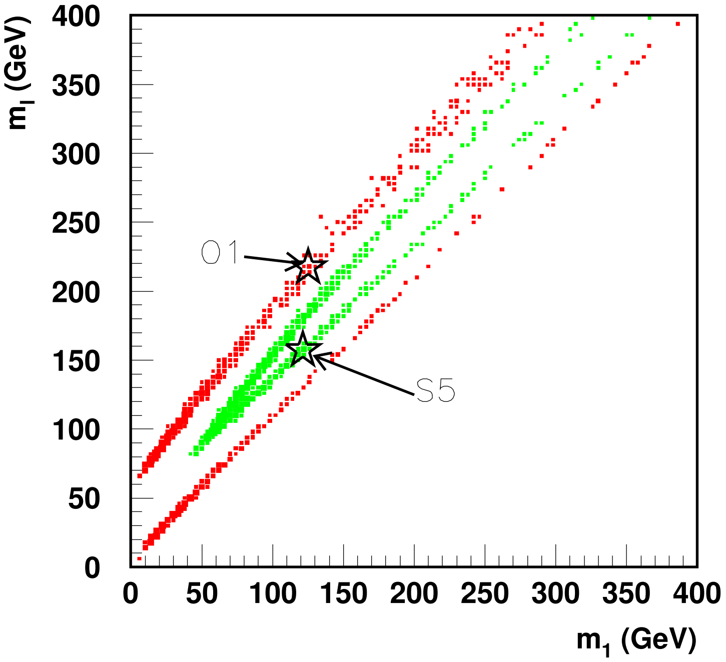

Figure 5.13: *The spread of* $\tilde{l}_R$ *and* $\tilde{\chi}_1^0$ *masses reconstructed by an ensemble of simulated ATLAS experiments, each using a cut-down version of the "basic" analysis (see Section 5.12) in which no use was made of the* l^+l^-q *threshold. Note how the overall mass scale here is constrained mush less than in Figure 5.12. Colours as in Figure 5.12.*

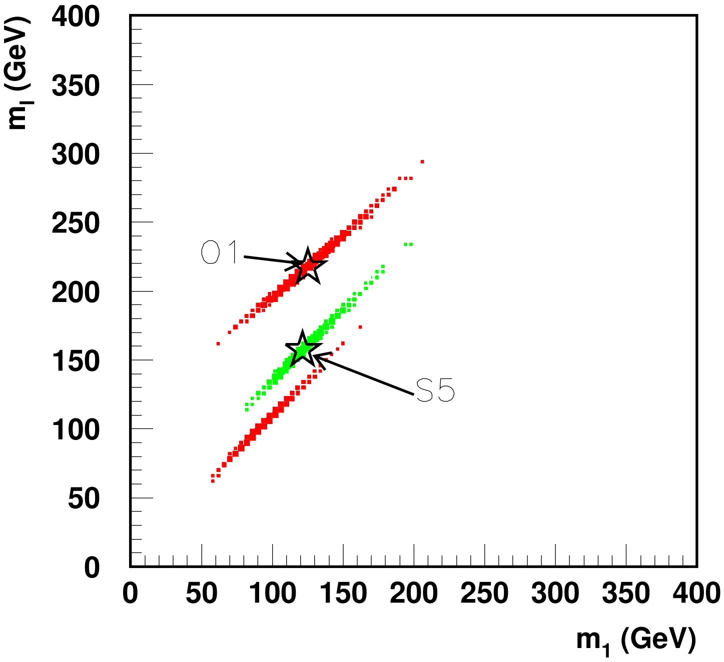

Figure 5.14: *The spread of* $\tilde{l}_R$ *and* $\tilde{\chi}_1^0$ *masses reconstructed by an ensemble of simulated ATLAS experiments, each using the "extended" analysis (see Section 5.13). Colours as in Figure 5.12.*

the overall mass scale at second order. It is thus possible to confirm one of the claims of [25–27], that the introduction of the l^+l^-q threshold is crucial in fixing the overall mass scale.

5.13 Extended reconstruction

An "extended analysis" may be defined by incorporating the novel $l^{\pm}q$ low-edge within the basic analysis of the previous section. The extended analysis thus makes maximal use of the boost invariant edges described in this thesis.

Figure 5.14 shows the reconstruction regions obtained after an application of the extended analysis at the two test points. As always, there remains a strong correleation between reconstructed slepton and neutralino masses. However, the reconstruction is clearly much improved by the inclusion of the new edge. Not only is the overall mass scale now much better constrained (the regions are smaller) but crucially, the undesired high slepton-mass region has disappeared entirey at S5. At O1 the improvement consists only of the improvement in resolution, as the undesired low slepton-mass region still remains.

Although the results are presented in terms of an *ensemble* of experiments, a *single* experiment observing edges like those of S5 would also find only one region of the $m_{\tilde{\chi}_1^0}$-$m_{\tilde{l}_R}$ plane consistent with the edge positions. Effectively this means that, for S5, the analysis can stop at this point. This is not to say that the smallest possible sparticle mass errors have been achieved yet; the point is only that the probability distribution for reconstructed masses is now approximately gaussian (and centred on the correct values) rather than spread over two disconnected regions. Indeed, it will shortly be seen that further analysis at S5 (using $\Delta M^{\max}$) can in fact produce a valuable new result. Nevertheless, the difference in character between the "single consistent region" of S5 and the "pair of consistent regions" remaining at O1, mean that the way subsequent results are *interpreted* will differ in the two cases. It will be possible to make stronger claims when faced with edges like those of S5, where the problem is already better constrained.

In order to remove the ambiguities associated with the correct evaluation of $m_{\tilde{l}_R} - m_{\tilde{\chi}_1^0}$, it is necessary to introduce the $\Delta M^{\max}$ observable.

5.14 Reconstruction using $\Delta M^{\max}$

Up to this point, edges have made definite (albeit ambiguous) statements about $m_{\tilde{\chi}_1^0}$, $m_{\tilde{\chi}_2^0}$, $m_{\tilde{l}_R}$ and the squark mass scale $m_{\tilde{q}}$. As we have already seen, the ΔM edge is not so kind to us. While we are able to measure the position of the principal ΔM edge to $\sim 10\%$, we cannot be sure (from the edge alone) whether it is due to light ($\tilde{l}_R$) or heavy

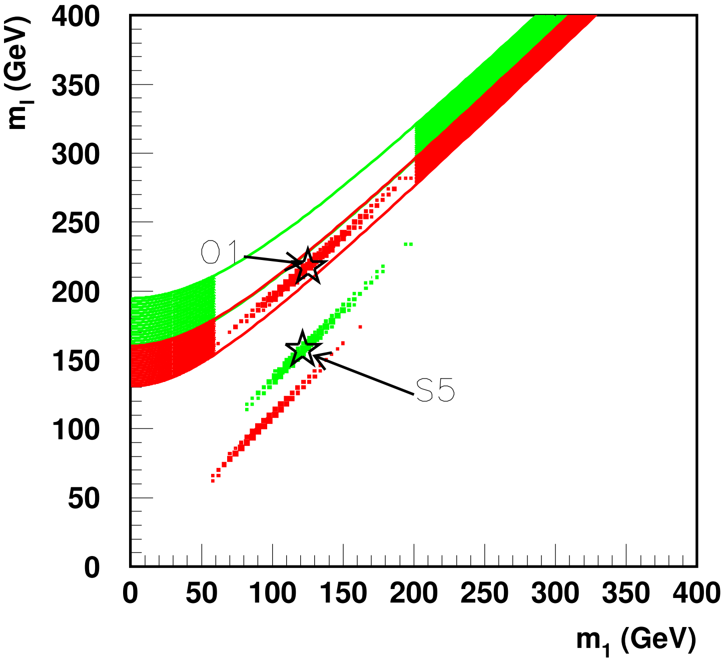

Figure 5.15: *The ΔM constraint. This figure is identical to Figure 5.14, except that it also shows the one-sigma regions favoured by 10% measurement of the "principal ΔM edge" in each of the two models. A window has been left in the centre section of each of the one-sigma regions so that they do not obscure the underlying scatter points. Colours as in Figure 5.12.*

($\tilde{l}_L$) sleptons. This can be both a blessing and a curse.

The best situation to find oneself in is one in which "other" measurements have already determined $m_{\tilde{l}_R} - m_{\tilde{\chi}_1^0}$ to some precision, while at the same time the ΔM edge is seen to favour an even larger lepton/neutralino mass difference. In these circumstances one has a strong claim to have obtained exciting and compelling evidence for a new heavier slepton (which we will identify with $\tilde{l}_L$) whose relation in mass to the mass of the LSP may be inferred from the location of the ΔM edge. We are fortunate enough to find ourselves in this position at S5. This may be seen in Figure 5.15, which shows the scatter points from the "extended analysis" (of the last section) overlaid with the region favoured by a 10% measurement of the "principal ΔM edge". The region favoured by the ΔM measurement is seen to lie many standard deviations above the region determined by the preceeding analysis. Far from signalling inconsistency, this information is welcomed as a sign that the ΔM measurement has managed to measure the mass of the as-yet-undiscovered left-slepton. The mass it attributes to the left-slepton has a central value given by $m_{\tilde{l}_L} = \Delta M^{\max} + \sqrt{m^2_{\tilde{\chi}_1^0} + (\Delta M^{\max})^2}$ where $\Delta M^{\max} = 88.5$ GeV ± 10% for the principal edge at S5.

At O1 the situation is somewhat different. Firstly, as has already been mentioned, the extended analysis generates two regions in the sparicle mass plane which are consitent with the observed edges at O1. Secondly, the masses favoured by the ΔM edge at O1are not "inconsitent" with the results of the earlier analysis (as was the case at S5). On the contrary, they actually overlap the upper of the two remaining regions, as Figure 5.15 shows. Being in the priviledged position of knowing what the montecarlo was instructed to generate, the coincidence does not surprise us; after all, *we* know that the lower region is the "fake" while the upper region and the ΔM constraint are both measurements of $m_{\tilde{l}R}$. Putting this knowledge to one side, however, what is our position?

If the ΔM constraint had fallen *between* the two regions (or on top of the lower one) we could have immediately accredited it with haveing both measured the mass of a heavy slepton, while at the same time settling the ambiguity associated with the interpretation of the two regions. Even if the ΔM edge constraint had fallen above the upper region, we could still have claimed a measurement of a heavy slepton's mass, even if the ambiguity of the concerning the lighter slepton's mass remained unsolved. However, the place at which the ΔM constraint *does* fall at O1 is the most tantalising. It tells us only one thing outright, namely that there is at least one slepton with a mass lying in the region covered by the ΔM constraint. What we do not learn is

- whether the consistency with the upper region entitles to rule out the lower region (thus letting us claim aa "double" measurement of the light slepton mass, with consequently improved errors);
- whether the consistency is just an accident; a "chance coincidence" between "a ΔM constraint favouring a heavy slepton mass" and "an unphysical region of parameter space which was regrettably not ruled out by the earlier analysis". In this situation we would regarn the lower O1 region as a measurement of the light-slepton mass; or
- whether the light and heavy sleptons might both be degenerate in mass (or nearly so) at the value indicated by the upper region and the ΔM constraint taken together.

The situation at O1 is clearly not "pretty" but it may at least be summarised in a positive way: the good news is that at O1 we either obtain an *improved* measurement of the light slepton mass (while learning nothing about heavier sleptons) or we are able to claim measurement of both light and heavy slepton masses. The catch is that the edges alone (at the given resolutions) cannot distinguish between these two possibilities.

What methods might we use to resolve the interpretation issues arising in connection with the slepton masses at O1? The first and most obvious suggestion os to try to use information from cross sections. Since we need to resolve problems with slepton masses, dislepton production would appear to be the production process we need to study. But unfortunately, the cuts which the counting of dislepton events require are basically those used to obtain events for the ΔM edge. We have alredy seen that these cuts are fine for counting events containing sleptons which are heavy enought to produce ΔM values that may be seen above the SM backgrounds, but these are precicely the events we are *not* interested in. The principal ΔM edge aready gives us an estimate of such slepton masses which is likely to be more reliable (less model dependent) than one derived from a counting argument using the same evetns. Our problem is not that we do not know the value of *this* slepton mass, but that at O1 we are unsure about wether there us a *lighter* slepton at the mass suggested by the lower of O1's regions in Figure 5.15. Using cross sectional information to weigh such a lighter slepton requires the use of cuts that are able to pull out a signal of the suze and shape of S5's light slepton events (Figure 5.8(a) and (b)) from underneath the SM backgrounds which are two orders of magnitude larger (Figure 5.9), and there is no evidence to suggest that such cuts are likely to be forthcoming.

If cross sections are to be abandoned in the search for possible means to remove the remaining issues at O1 we are left with: branching ratios, the use of new decay chains, and the creation of new observables for existing chains. All the options will be left for future investigations, although it is remarked that the possibilities for forming more "artificial" edges (like the l^+l^-q threshold, which we recall is but one of an otherwise unexplored family of edges governed by the choice of lower limit for m_{ll}) have by no means been exhausted yet.

that $p < q$ is the condition for $m^{\max}_{l_{\text{near}}q}$ to be added to the list of possible candidates for $m^{\max}_{lq(\text{low})}$. Note however, that the condition controlling its inclusion is precisely the condition which causes it to be added under "Case 1" anyway. Therefore "Case 2" adds no new information and may be ignored.

Case 3

There is only one unconstrained local maximum for $m_{l_{\text{far}}q}$, and it occurs when the quark is pointing along l_{near} and back-to-back with l_{far} in the rest frame of the slepton. Note that, in contrast with "Case 2" all the momenta are now fixed. Moreover, this configuration has fixed $m_{l_{\text{near}}q} = 0$, which means that $m_{l_{\text{far}}q}$ in this state is most certainly not smaller than $m_{l_{\text{near}}q}$. Thus "Case 3" generates no masses at all.

Summary

Putting all the results together, the following result is obtained:

$$(m^{\max}_{lq(\text{low})})^2 = \begin{cases} (m^{\max}_{l_{\text{near}}q})^2 & \text{when} \quad p \leq q \\ \frac{(c-b)(a-z)}{2a-z} & \text{when} \quad p \geq q. \end{cases} \tag{D.36}$$

D.7 $\tilde{l}\bar{\tilde{l}}$ edge

It was mentioned in Section 5.7.6 that the condition for a event to yield a value of $M_{T2}(\chi)$ close to the maximum is that $\Delta y_1 = \Delta y_2 = 0$ and $\mathbf{v}_T^{l_1} - \mathbf{v}_T^{\tilde{\chi}_1}$ is parallel (note: not anti-parallel) to $\mathbf{v}_T^{l_2} - \mathbf{v}_T^{\tilde{\chi}_2}$. The definitions of Δy_i and $\mathbf{v}_T^{X}$ may be found by referring back to Section 5.7.6. To establish the value of $M_{T2}^{\max}(\chi)$ it is thus sufficient to calculate the value of $M_{T2}(\chi)$ in an event satisfying the condition. The simplest such event contains two sleptons, at rest in the frame of the detector, and with each decaying into a lepton travelling along the negative x-axis and a neutralino along the positive x-axis. In the frame of the sleptons, both the neutralino and the lepton will have a three momentum $\mathbf{p}$ with modulu p satisfying

$$p^2 = \frac{m_{\tilde{l}}^4 + m_{\tilde{\chi}_1^0}^4 + m_l^4 - 2(m_{\tilde{l}}^2 m_{\tilde{\chi}_1^0}^2 + m_l^2 m_{\tilde{\chi}_1^0}^2 + m_{\tilde{l}}^2 m_l^2)}{4 m_{\tilde{l}}^2}. \tag{D.37}$$

In order to calculate $M_{T2}(\chi)$ in accordance with Definition (5.13) we need to evaluate

$$M_{T2}^2(\chi) \equiv \min_{\not{\mathbf{p}}_1 + \not{\mathbf{p}}_2 = \not{\mathbf{p}}_T} \left[\max\left\{m_T^2(\mathbf{p}_T^{l_1}, \not{\mathbf{p}}_1, \chi), m_T^2(\mathbf{p}_T^{l_2}, \not{\mathbf{p}}_2, \chi)\right\}\right]. \tag{D.38}$$

For the particular configuration described above we can say that

$$\begin{aligned} m_T^2(\mathbf{p}_T^{l_1}, \not{\mathbf{p}}_1, \chi) &= \chi^2 + m_l^2 + 2\left(\sqrt{m_l^2 + p^2}\sqrt{\chi^2 + (p+\delta)^2 + q^2} + p^2 + p\delta\right) & \text{(D.39)} \\ m_T^2(\mathbf{p}_T^{l_2}, \not{\mathbf{p}}_2, \chi) &= \chi^2 + m_l^2 + 2\left(\sqrt{m_l^2 + p^2}\sqrt{\chi^2 + (p-\delta)^2 + q^2} + p^2 - p\delta\right) & \text{(D.40)} \end{aligned}$$

where $\not{\mathbf{p}}_1$ and $\not{\mathbf{p}}_2$ have been parametrised by the two real numbers δ and q according to

$$\not{\mathbf{p}}_1 = \begin{pmatrix} p+\delta \\ q \end{pmatrix} \qquad \text{and} \qquad \not{\mathbf{p}}_2 = \begin{pmatrix} p-\delta \\ -q \end{pmatrix} \tag{D.41}$$

in order to ensure that $\not{\mathbf{p}}_1 + \not{\mathbf{p}}_2 = \not{\mathbf{p}}_T$ is automatically satisfied. Note that we may choose both $q \geq 0$ and $\delta \geq 0$ without loss of generality, and having done so we may then deduce that the right-hand-side of (D.39) is always greater than or equal to the right-hand-side of (D.40). With this fact in mind, the two values of m_T may be substituted into (D.38) yielding

$$M_{T2}^2(\chi) = \min_{q \geq 0, \delta \geq 0} \left[\chi^2 + m_l^2 + 2\left(\sqrt{m_l^2 + p^2}\sqrt{\chi^2 + (p+\delta)^2 + q^2} + p^2 + p\delta\right)\right]. \tag{D.42}$$

Minimisation over q is trivial and is achieved by setting $q = 0$. The derivative with respect to δ of the argument of the "max" in (D.42) may also be evaluated, and can be shown to be positive. The minimisation with respect to δ is thus achieved by setting δ also equal to zero. We now have all that is required to determine $M_{T2}(\chi)$ for this particular configuration, which by design provides us with the general formula for $(M_{T2}^{\max}(\chi))^2$:

$$(M_{T2}^{\max}(\chi))^2 = \chi^2 + m_l^2 + 2p^2 + 2\sqrt{m_l^2 + p^2}\sqrt{\chi^2 + p^2}, \tag{D.43}$$

from which we observe that

$$M_{T2}^{\max}(\chi) = \sqrt{m_l^2 + p^2} + \sqrt{\chi^2 + p^2}. \tag{D.44}$$

Notice that if χ is set equal to the real neutralino mass, $m_{\tilde{\chi}_1^0}$, then we recover the expected result $M_{T2}^{\max}(m_{\tilde{\chi}_1^0}) = E_l + E_{\tilde{\chi}_1^0} = E_{\tilde{l}} = m_{\tilde{l}}$. In passing I remark

D.8 NOT A HIGH PRIORITY BUT ...

XXX If desired, at this point I could include a description of a general edge finding process for finding $m_{abc\ldots xyz}^{\max}$ for the chain $A \to aB, B \to bC, C \to cD$ ... . This would not be essential to the thesis though, XXX